Atomically-thin Single-photon Sources for Quantum Communication

Timm Gao,[1] Martin v. Helversen,[1] Carlos Anton-Solanas,[2] Christian Schneider,[2] and Tobias Heindel[1,*]

[1] *Institut für Festkörperphysik, Technische Universität Berlin, 10623 Berlin, Germany*

[2] *Institut für Physik, Carl von Ossietzky Universität Oldenburg, 26111 Oldenburg, Germany*

SUPPLEMENTARY INFORMATION

Photon arrival time distributions

For investigating the performance of the receiver module, the receiver's response to all four possible input polarization states is investigated. We sequentially prepare single photon pulses in horizontal (H), vertical (V), diagonal (D), and anti-diagonal (A) polarization. The events are detected at all four detectors and individually correlated with the laser synchronization signal to obtain time-resolved measurements. These are summarized in Fig. S1 on the left-hand side in a 4x4 matrix. The rows correspond to the input polarization and the column to the respective detection channel. Histograms within one row are normalized to the maximum of the input polarization (e.g., the first row is normalized to the maximum of the HH distribution (blue)). The matrix in the main text Fig. 2 (b) is calculated from the sum of each unnormalized matrix element in Fig. S1 divided by the acquisition time. Erroneous detection events can be made visible if the time-resolved measurement is renormalized to the arrival time probability distribution for both output channels in each basis, as depicted in the right panel of Fig. S1.

Temporal filtering

Fig. S2 depicts the QBER and the sifted fraction as a function of the width Δt of the acceptance time window ($t_\mathrm{c} = 0$) for each detection channel. The plots are calculated from the matrix elements in Fig. S1. Reducing

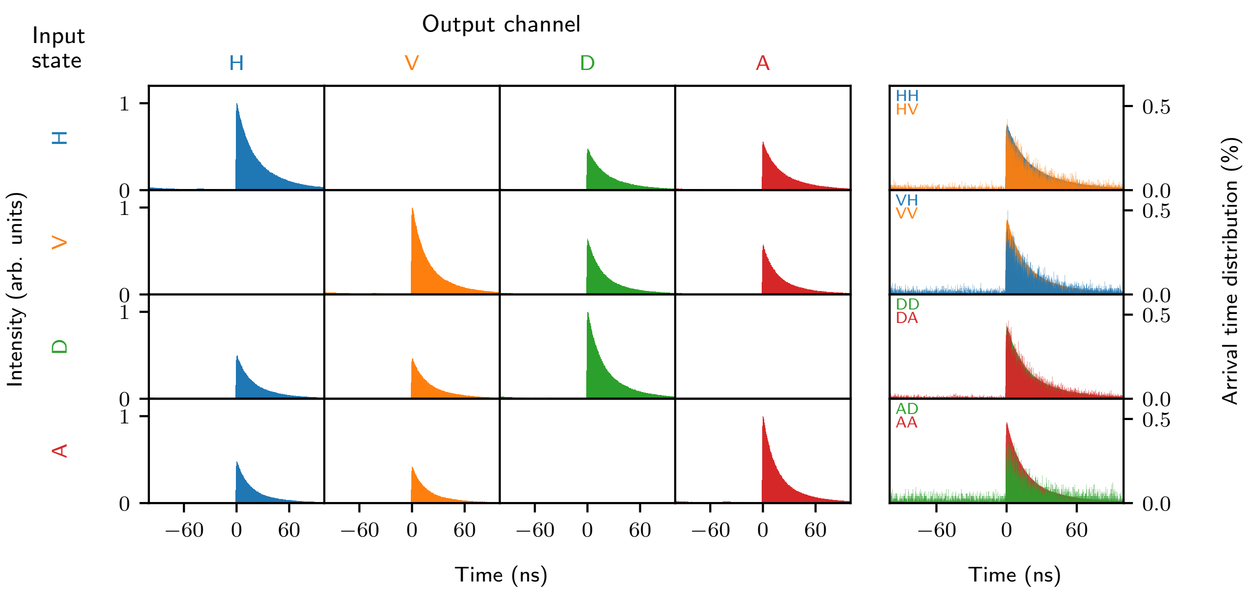

FIG. S1. Photon arrival time distributions measured at the receiver module. For each of the four possible input polarizations H, V, D, and A, the time resolved photoluminescence is measured at each of the four corresponding output channels of the receiver module individually. The time-bin width is 0.1 ns. The measurement data in the left 4x4 matrix is normalized to the maximum of the respective input state. The right panel shows the two data sets for a given input polarization basis (e.g., HH and HV). Here, each distribution is normalized to the sum of all events registered in the respective channel (e.g., the HV distribution is normalized by all clicks registered in the V-channel).

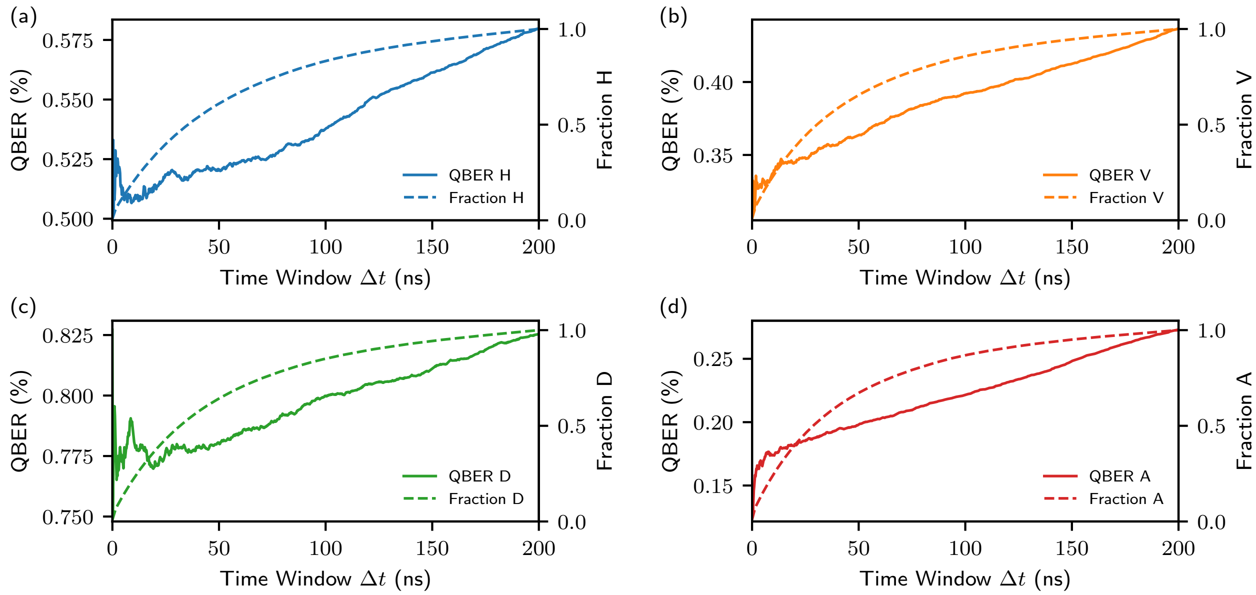

FIG. S2. Temporal filtering with fixed $t_c = 0$. (a) H input polarization. (b) V input polarization. (c) D input polarization. (d) A input polarization. From the photon arrival time distributions in Fig. S1 the QBERs and corresponding fractions of the sifted key are calculated depending on the width of the acceptance time window.

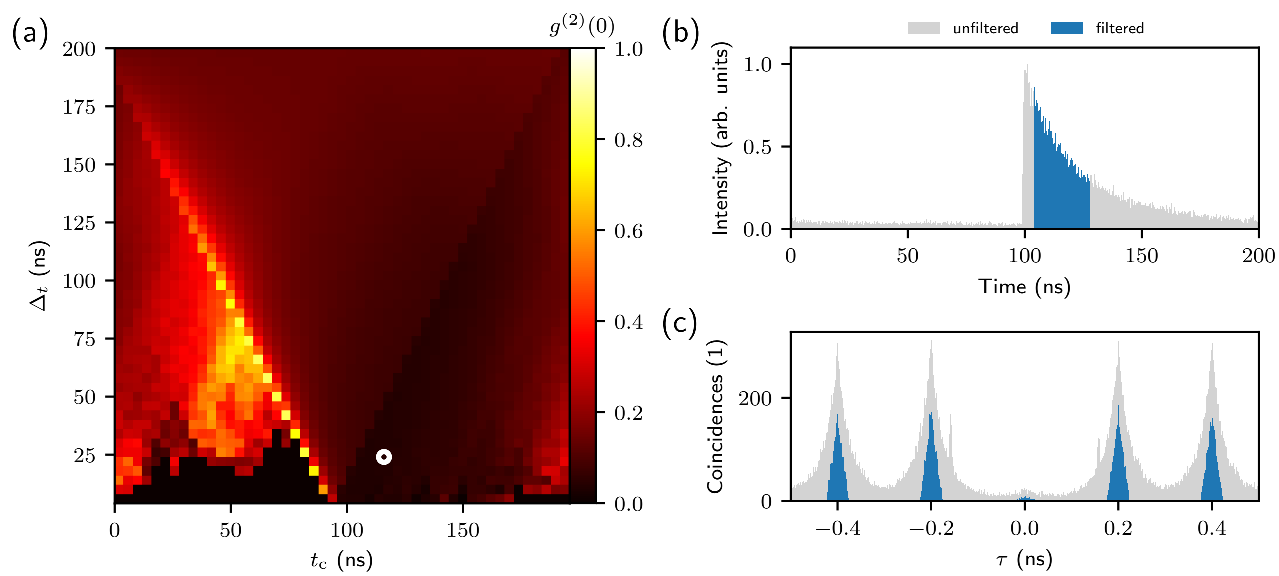

FIG. S3. 2D Temporal filtering of $g^{(2)}(0)$. (a) $g^{(2)}(0)$ as a function of the acceptance time window Δt and t_c. The $g^{(2)}(0) = 0.034 \pm 0.002$ from the main text is marked with a white circle ($\Delta t = 24\,\mathrm{ns}$, $t_c = 16\,\mathrm{ns}$). (b) and (c) Photon arrival time distributions and autocorrelation histograms for the unfiltered (grey) and filtered (blue) case corresponding to the parameter set marked in (a).

Δt, both the QBER and the sifted key fraction is reduced. The minimal QBER values reached are limited by optical imperfections in the experimental setup, as the contribution by detector noise are effectively discarded by the acceptance time window. The temporal filtering does however not only affect the sifted key fraction and QBER, but also the $g^{(2)}(0)$. While in QKD one cannot benefit from temporal filtering of $g^{(2)}(0)$ without adding modifications to the protocol implementation (see main text for details), we make use of it to estimate contributions limiting the single-photon purity. Figure S3 (a) shows the $g^{(2)}(0)$ of our WSe_2 single-photon source as a function of the acceptance time window Δt and t_c. For this we used a subset of the experimental data (corresponding to the first 15 min) from

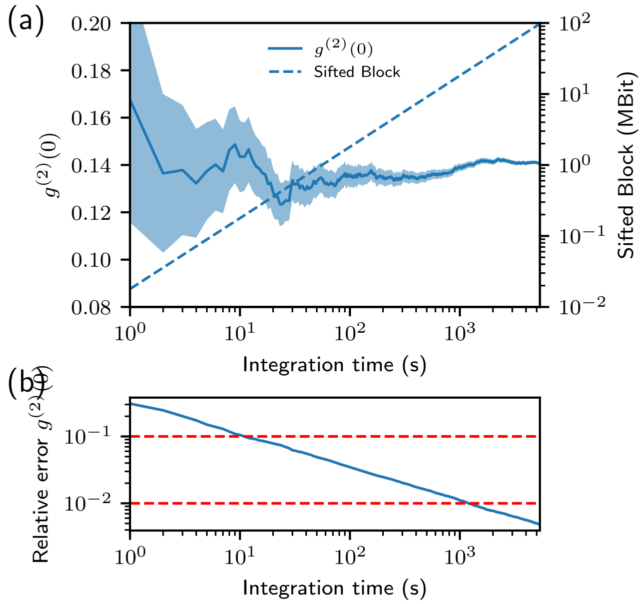

FIG. S4. Antibunching investigation over integration time. (a) The antibunching $g^{(2)}(0)$ of the SPS is evaluated via correlating the detection events of all for detectors in overlapping blocks for different accumulation times compared with the corresponding length of the sifted block. Here, the same dataset as in Fig. 2 (d) of the main text is used. (b) Relative error of $g^{(2)}(0)$ over the integration time.

the measurement presented in Fig. 2 (d) of the main text. For regions in black, i.e. zero, no reasonable $g^{(2)}(0)$ could be evaluated due to insufficient statistics. The minimum $g^{(2)}(0)$ is reached in the lower right quadrant of the 2D heatmap. In this region, signal from the exponential decay of the photon arrival time distribution of the quantum emitter is predominantly accepted, while residual background contributions of laser (left half, corresponds to rising edge of the photon arrival time distribution) and a large fraction of dark count contributions (lower left quadrant) is rejected. The white circle marks the value of $g^{(2)}(0) = 0.034 \pm 0.002$ at $\Delta t = 24\,\mathrm{ns}$, $t_c = 16\,\mathrm{ns}$ we state in the main text, being in good agreement with our estimate on the spectral background of 0.04 caused by uncorrelated background emission of the sample. This setting of the temporal filter results in a reasonable trade-off between the sifted key fraction (47 %) and the reduction of $g^{(2)}(0)$ from the unfiltered $g^{(2)}(0) = 0.139 \pm 0.002$. The photon arrival time distributions and corresponding autocorrelation histograms are shown in in Fig. S3 (b) and Fig. S3 (c) for the unfiltered (blue) and filtered (grey) case, respectively. While even lower $g^{(2)}(0)$ values can be achieved, tighter filtering leads to substantially reduced sifted key fractions. Comparing the two autocorrelation histograms in Fig. S3 (c), also reveals that there is a significant difference between correlating the filtered detection events instead of using a linear background subtraction and only a certain interval around each peak of the unfiltered histogram for evaluating $g^{(2)}(0)$.

Real-time photon statistics monitoring

For the real-time monitoring of the photon statistics, reasonable accumulation times need to be evaluated. In Fig. 2 (d) of the main text, we choose 10 s and 100 s. The choice of these accumulation times is based on Fig. S4 depicting the antibunching $g^{(2)}(0)$ of the our WSe_2 single-photon source as a function of the accumulation time. Here, the $g^{(2)}(0)$-value for accumulation times below 103 s is slightly lower even within the uncertainty bounds compared to the full measurement. This shows that a shorter acquisition time is suitable for taking changes in the emitter statistics into account. For 10 s accumulation time (0.178 Mbit sifted block size), the relative error is about 10 %, while an increase to 100 s (1.792 Mbit sifted block size) reduces the relative error below 5 %.

* Corresponding author: tobias.heindel@tu-berlin.de